ORTHOGONAL WAVE CURRENT INTERACTION OVER ROUGH BEDS: PRELIMINARY RESULTS OF THE WINGS HY+ TA PROJECT

Carla Faraci, Alessia Ruggeri, Giovanni Savasta (1), Rosaria E. Musumeci, Massimiliano Marino, Enrico Foti (2), Giuseppe Barbaro (3), Dag Myrhaug, Lars Erik Holmedal, Pierre-Yves Henry, (4), Paolo Blondeaux, Giovanna Vittori (5), Richard R. Simons (6), Bjarne Jensen, Bjorn Elsaβer (7)

(1) Department of Engineering, University of Messina, Italy, Email: cfaraci@unime.it
(2) DICAR, University of Catania, Italy, Email: rosaria.musumeci@unict.it
(3) Università Mediterranea di Reggio Calabria, Italy, Email: giuseppe.barbaro@unirc.it
(4) NTNU, Norway, Email: pierre-yves.henry@ntnu.no
(5) Università degli Studi di Genova, Italy, Email: blx@dicca.unige.it
(6) UCL, UK, Email: r.r.simons@ucl.ac.uk
(7) DHI, Denmark Email: bjj@dhi.dk

This paper reports some preliminary results obtained in the framework of the TA WINGS, funded by the EU through the Hydralab+ program. The project was aimed at gaining insights on orthogonal wave current interaction over rough beds. Velocity profiles were acquired within the DHI shallow water tank by means of several Vectrinos over sandy, gravel and rippled beds in order to investigate the effects of wave-current interaction on the bottom boundary layer and on the bed shear stresses.

1. INTRODUCTION

Wave-current interaction strongly affects the nearshore hydrodynamics, inducing changes both in the mean velocity profile and in the turbulent characteristics, in the structure of the bottom boundary layer and in the bed shear stress. Since the hydrodynamics at the bottom of the sea wave plays a fundamental role on many phenomena such as sediment transport, diffusion, mixing process, etc., the relevance of the topic in the coastal research community is unquestionable.
Following this consideration, in the last decades many experimental studies have been devoted to investigate wave-current bottom boundary layers in the case of currents following or opposing the waves (Kemp and Simons 1982,1983, Lodahl et al., 1998) or orthogonally interacting one with each other (Musumeci et al., 2006, Faraci et al., 2008, Lim et al., 2012). According to some of these studies, a key role in the wave current interaction seems to be played by the ratio between current and wave orbital velocity. Indeed, when the flow field is dominated by the current (current-dominated regime), a linear interaction occurs between the two forcing, while if the wave contribution prevails (wave-dominated regime) the nature of the boundary layer also play an important role.
Musumeci et al. (2006) found that when waves are added onto a current over a bed characterized by a small roughness, an increase of the current flow at the bed occurs; the contrary occurs in the case of large roughness.
The case of a rippled bed is also similar to a large roughness, causing the wave boundary layer to become turbulent and the bed roughness to increase up to an order of magnitude when waves are superimposed to a current (Fredsøe et al., 1999; Faraci et al., 2008). More recently, Faraci et al. (2018) shed also light on the statistical nature of the waves plus current near-bed velocities. They observed that the combined wave-current velocity distribution is double-peaked and can be decoupled in order to get single-peaked velocity distributions splitting the data in two classes according to the sign of the wave directed velocities.
In this work, both current and wave dominated conditions were investigated in order to understand the nature of the velocity distribution along the water column and the apparent bed roughness as well as the structure of the bottom boundary layers.

The effects of three different rough beds (sand, gravel, fixed ripples) on the velocity distribution along the water column were considered.
This task was accomplished within an experimental campaign carried out in the framework of the Transnational Access WINGS - Waves plus currents INteracting at a right anGle over rough bedS, funded by the EU Commission through the Hydralab+ program.
In this paper, some of the results of this campaign on the three different rough beds (briefly indicated as SB, GB and RB) are discussed and compared. The paper is organized as follows: first the experimental set up and instrumentation is presented, then the experiments are reported and the experimental results are discussed. The paper ends with some conclusions.

2. EXPERIMENTAL SET UP

2.1 Shallow water basin

The experimental campaign was carried out at the Shallow Water Tank at DHI (Horsholm, Denmark). The tank dimensions are *35 m* by *25 m* (Figure 1). Along the longer side of the basin, the propagation of a current is generated by three submerged pumps, able to recirculate on the complex a flow rate of *1* m^3/s. The inlet section was reduced from *25 m* to *12 m*, in order to reproduce both current dominated and wave dominated regimes.
In Figure 1a*)* a sketch of the shallow water tank is reported. The origin of the reference system is located in the lower left corner of the basin and it is identified in Figure *1* with *O*; the *x*-axis follows the current direction, while the *y*-axis is directed as the wave propagation direction. *z*-axis has the origin at the bottom and points upward.
Waves are generated by a wavemaker 18 m wide, obtained by an array of 36 piston-type wave paddles, 1.2 m high and 0.5 m wide each.
Each paddle is controlled by an electric-servo motor through software DHI *WaveSynthesizer*, allowing the wave type (regular or random), the water depth, the wave characteristics and the test duration to be set up.
The *3D* wave generator is designed to operate at water depths *D* between *0.2 m* and *0.8 m.*
A C-shaped gravel beach with a slope of *1/5.6*, coupled with passive parabolic wave absorbers, provides energy absorption at the opposite end of the wave basin.
In this experimental campaign the tests were carried out with three beds with different roughness. In particular, several panels, each one measuring *1.25 x 2.5 m* were used to control bottom roughness over an area of *37.5* m^2. Namely a sandy bed (SB), a gravel bed (GB) and a rippled bed (RB) were installed in the wave-current interaction area of the basin.
The first two beds were obtained by gluing sand (d_{50}*=0.9-1.6 mm*) or gravel (d_{50}*=16-32 mm*) on wood tiles, which were thus drilled on the concrete floor in order to be fixed.
The rippled panels were built by fixing on the floor corrugated plastic panels having proper dimensions (height *1.85 cm* and wavelength *12.5 cm*) through screws of dimensions *4 x 3.5 mm*. Subsequently a homogeneous layer of glue was distributed and the ridges of the ripples were created with the use of a wooden template. Finally, they were sprinkled with the same sand of the sandy panels in order to reproduce proper surface roughness.

2.2 Instrumentation

A set of *24* resistive wave gauges, located in the central part of the basin where waves and currents interact orthogonally with each other, allowed the free surface to be recovered (Figure 1b). Five of them were placed along the same *x*-line and shifted along the *y*-axis by a fixed interval in order to measure the wave reflection inside the basin according to the method of Faraci et al. (2015).
Velocity profiles were acquired by means of several high resolution Acoustic Doppler Velocitimeters (Vectrino produced by Nortek As.). More in details, five Single-Point Vectrinos (*VS*), four of them down-looking and one side-looking, and one Vectrino Profiler (*VP*) were employed in the present experimental campaign.
Over the sandy and gravel bed, four *VS* were placed in a square shape, whose side was equal to *0.12 m*, while one *VS* occupied the centre of the square.
In the rippled bed tests, the cross configuration of the set of the Single-Point Vectrinos was modified and the instruments were displaced along the same line at a right angle with respect to the ripple crest. The Side Looking Vectrino was retreated by 5 cm with respect to the other four.

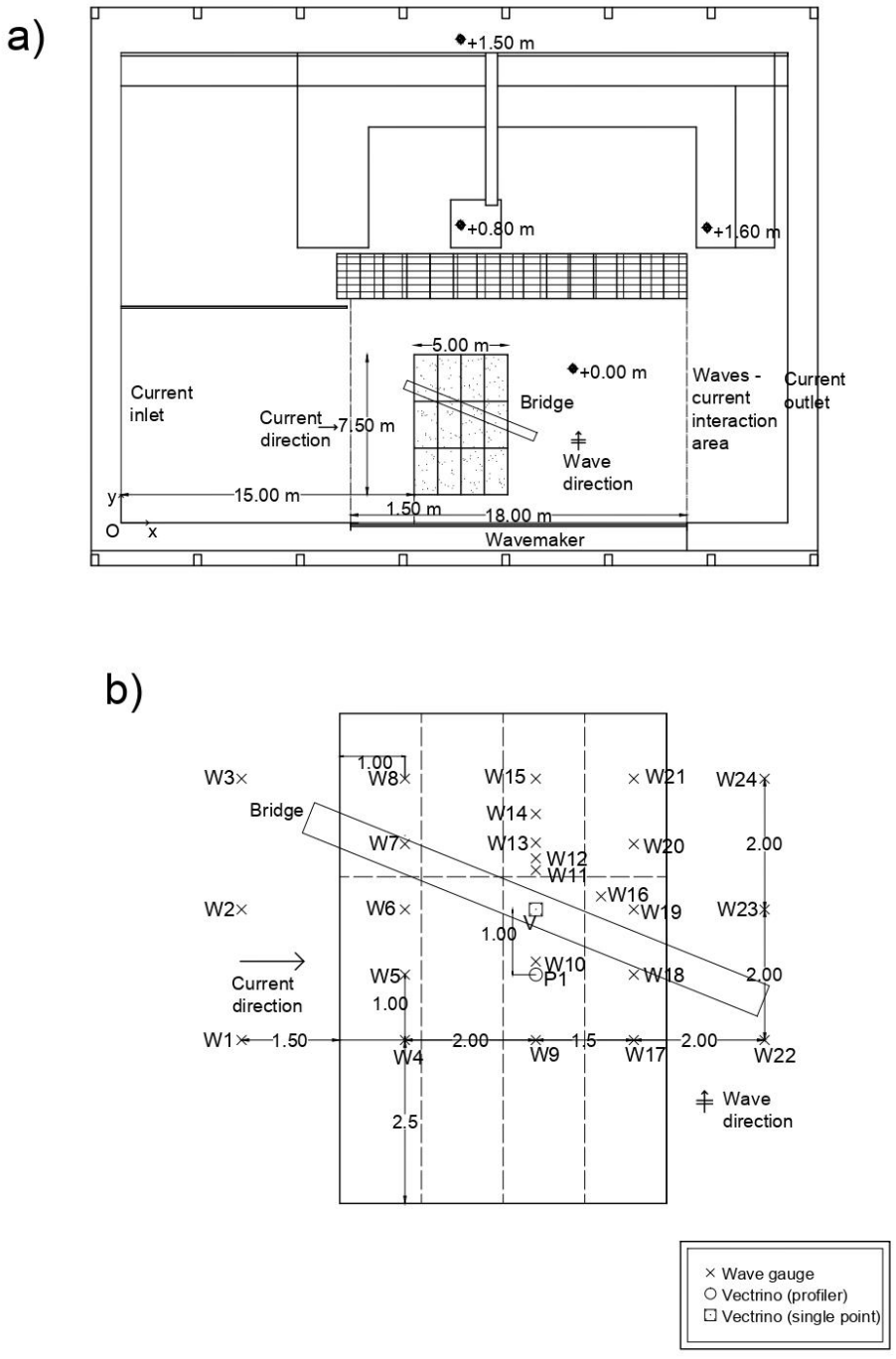

Figure 1. (a) Sketch of the DHI shallow water basin; (b) Zoom of the wave-current interaction area and instrument location inside the basin during the WINGS experiment.

Moreover, for rippled bed, in order to increase the number of vertical velocity profiles along the ripple profile including crest and trough, two different measurement positions were used by shifting the trolley of *1/8* of ripple wavelenght. The position of the Vectrinos for sandy or gravel bed and ripples bed is indicated in Figure *2*.

The whole system was held by a trolley mounted on a bridge and vertically moved by means of a micrometer.

The sampling volume of the VS probe is located 50 mm far from the transducer and its dimensions can be modified via the acquisition software in relation to the desired quality of the signal; the sampling rate is up to 200 Hz. The sampling volume of the VP probe extends from 40 mm down to 74 mm below the transducer, typically divided into 34 measuring cells with 1 mm resolution and sampling rate equal to 100 Hz.

The position of VSs and VP was set on the basis of preliminary tests focused on the definition of an area inside the basin where both waves and currents maintain a steady state, as it will be shown in the next section.

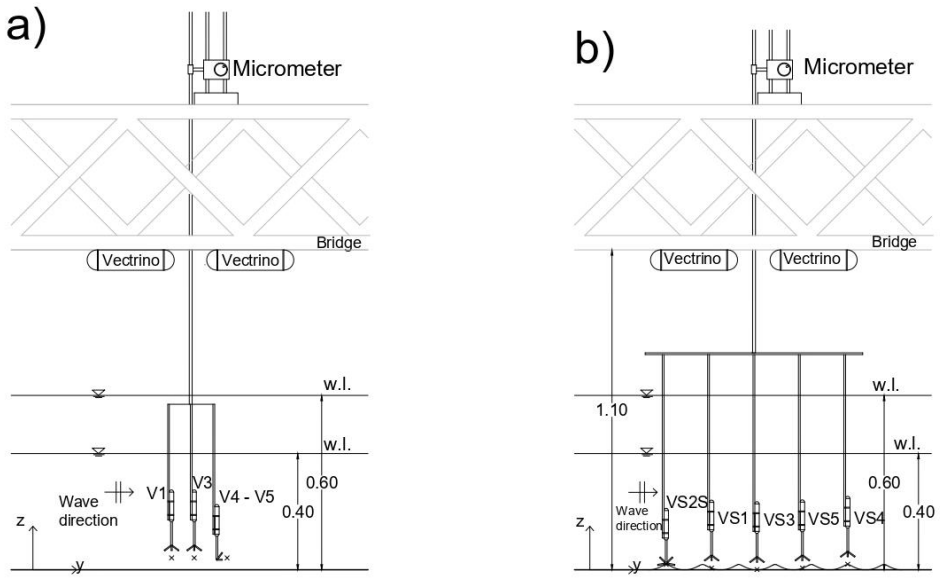

Figure 2. (a) plan view of the Vectrino Single Point position (SB and GB);
(b) plan view of the Vectrino Single Point position (RB).

The reliability of the measured velocities is related to two parameters namely Correlation (COR) and Signal to Noise Ratio (SNR), (see e.g.van der Zanden et al., 2017; Yoon and Cox, 2010). Two acceptance thresholds were adopted: *COR ≥ 90* and *SNR ≥30* near the sweet spot, i.e. from 50 to *65 mm* below the transceiver, *SNR ≥ 20* elsewhere. Non-reliable data were replaced by linear interpolation. Finally, data were despiked by means of the Goring and Nikora (2002) method.

Profiles acquired by the VP were obtained by vertically overlapping each measurement station by a certain amount. This is necessary in order to be able to remove the lower part of the sampling volume data, characterized by low SNR because of sound reflection from the bottom, without producing any gap in the profiles. When vertically moving from a position to another along the profile, the sensor position is shifted up by an amount Δz in each run. In order to get the proper overlap between two successive stations, Δz was kept equal to *2 cm*. For sake of brevity, data acquired by VP are not displayed in the present paper.

Wavemaker, wave gauges and Vectrinos are all synchronized by means of a TTL (*Transistor-Transistor-Logic*) and acquired by means of a data logger.

In Figure 1b a plan view of the position of the instruments inside the basin is reported.

In Table *1* the position of single point Vectrinos and Vectrino Profiler within the tank are reported for SB, GB and RB.

Table 1. Position of the Vectrinos for the sand, gravel and ripples bed.

Instrument name	Reference	SB and GB		RB	
		x [m]	y [m]	x [m]	y [m]
Vectrino profiler 1	VP1	18	5	18	5
Vectrino profiler 2	VP2	19	6	//	//
Vectrino single point 1	VS1	17,88	6	18	5,84
Vectrino single point 2	VS2	18	5,88	18,05	5,69
Vectrino single point 3	VS3	18	6	18	6
Vectrino single point 4	VS4	18	6,12	18	6,31
Vectrino single point 5	VS5	18,12	6	18	16

3. EXPERIMENTS

Waves with periods between *1* and *2 s* and wave heights between *0.05 m* and *0.12 m* were propagated along the basin.
Two different water depths *d* were considered, *0.4* and *0.6 m*. In this way two different current conditions were generated within the flume keeping the flow rate equal to 1 m^3/s.
The combination of the wave and the current conditions led to reproduce both wave-dominated and current-dominated regimes.
Some preliminary tests were performed in order to check the regularity of the flow within the test area and to determine both the location of the rough panels inside the basin and the position of the instrumentation. First a Lagrangian particle tracking analysis, carried out using neutrally buoyant particles, allowed the large scale wave-current interaction to be monitored and secondary flows to be investigated by means of visual inspection. One water depth (*d=0.4 m*), i.e. one current condition, and one wave condition (*H=0.12 m* and *T=2 s*) were selected in order to run these preliminary tests. After that, a map of the flow conditions within the basin at one vertical position located *0.1 m* from the bed was carried out by means of one Vectrino single point. A current only case and a wave plus current one were taken into account. The main goal was to check to what extent the velocity in the outer flow could be influenced by the local coordinate. The measurements explored almost the entire area where the waves interact with the current; *14* measuring points in the current only case and *12* points in the wave plus current case (*5 m< x <30 m; 3.5 m< y < 8.5 m*) were acquired .
Moreover, before starting with the actual test programme, a time convergence test was performed, i.e. the velocity components were acquired at one point for *30* minutes and the convergence of the first and second order statistics were analysed by considering a different acquisition time. Moreover the comparison of the ensemble average with the single waves allowed to assess that no visible differences occurred within the acquisition time.
The results of these preliminary tests therefore allowed to define both the optimal position of the measurement point for the detailed investigations concerning the hydrodynamics generated by waves and currents on rough surfaces, as well as the time duration of the tests. As a result, it was decided to place the measuring point for the acquisition of the velocity profiles at the coordinate point *x = 18.5 m, y = 6 m.*
During the experimental campaign a total of 67 runs were performed, 18 of which for SB, 18 for GB and 31 for RB respectively (Table 2).
More in detail, for SB and GB cases, two runs of current only (CO) (*d=0.4 m and d=0.6 m*), 8 of waves only (WO) and 8 of waves and current (WC) were made, changing the period and the wave height (*T=1 s and T=2 s* and wave height between *H=0.12 m* and *H=0.05 m*).
For the rippled bed case, 18 runs were performed for the first trolley position, two of which were only current (CO), 8 of waves only (WO) and 8 of waves and currents (WC).
For the second position of the trolley, five runs of waves only (WO), two of only current (CO) and six of waves and current (WC) were carried out by changing wave height and period.

Table 2. Overview of the test conditions for respectively SB, GB and RB case.

Flow cond.	D(m)	Flow cond.	H(m)	T(s)	Flow cond.	H(m)	T(s)
CO	0,4	WO	0,05	1	WC	0,05	1
			0,08	1		0,08	1
			0,08	2		0,08	2
			0,12	2		0,12	2
	0,6		0,05	1		0,05	1
			0,08	1		0,08	1
			0,08	2		0,08	2
			0,12	2		0,12	2

4. ANALYSIS OF THE EXPERIMENTAL RESULTS

4.1 Water surface

Regular waves were measured by the wave gauges during all the tests. An example of the acquired signal is reported in Figure *3*, where the ensemble average is plotted above each single recorded wave in the cases of different roughness: Run 16 (SB), Run 25 (GB) and Run 48 (RB) (*d=0.6 m; H=0.08 m; T=1 s*).
The wave signal seems to be fairly regular and with a good repeatability. Moreover, the comparison of overlapped waves for the three bed roughness shows a higher variability for the case of ripples. More in details, the average crest - trough variability estimated as the displacement of the maximum crest elevation or minimum trough position with respect to the ensemble average was found to be equal to 9.6%, 8.7% and 15.3% respectively for SB, GB and RB.

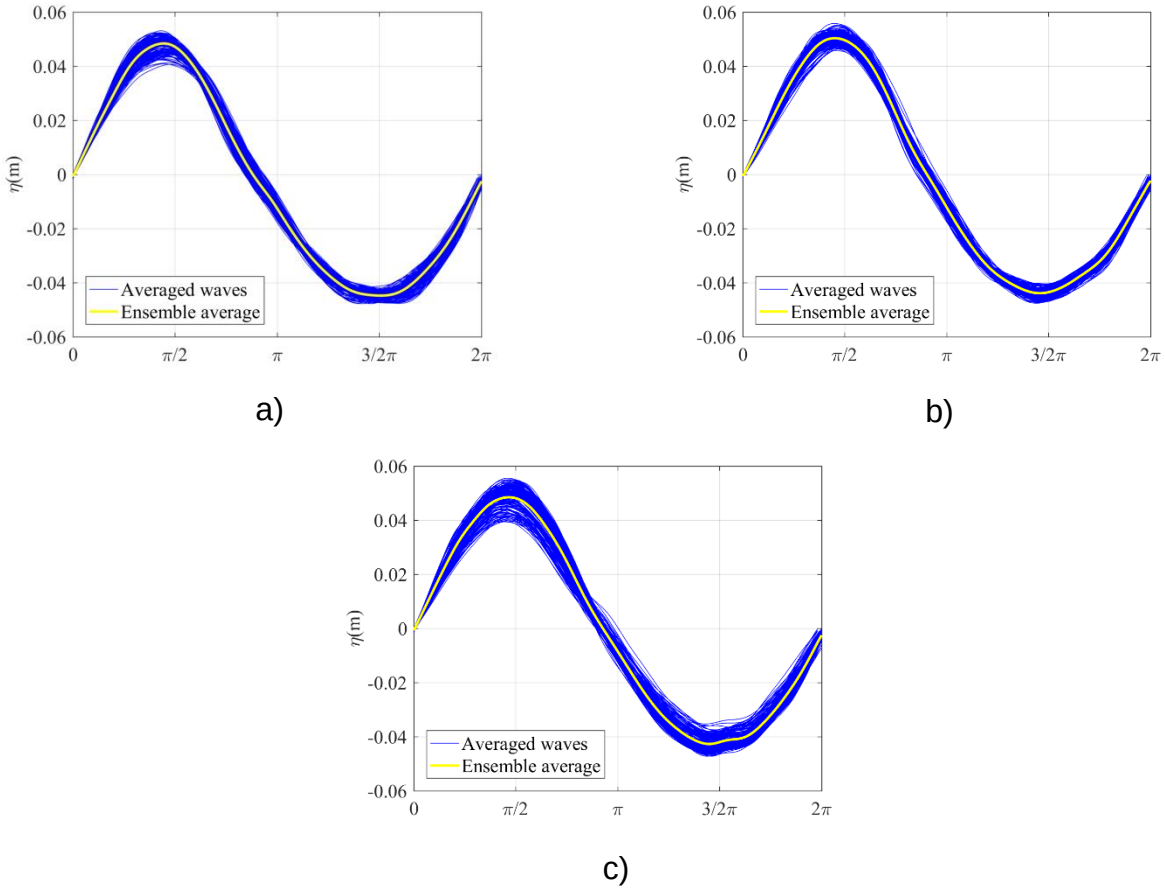

Figure 3. Wave series acquired during (a) Run 16 (SB), (b) Run 25 (GB) and (c) Run 48 (RB) (*d=0.6 m; H=0.08 m; T=1 s*)

4.2 Mean velocity profiles and shear stresses

In this section mean velocity profiles acquired by Single Point Vectrinos are shown.
As mentioned before, for each test the velocity was acquired by means of several Vectrinos, which were then averaged in order to obtain a spatially averaged velocity.
An example of this procedure is shown in Figure *4*, where the velocities acquired by each Vectrino in three current-only tests characterized by a water depth d=*0.4 m* and by different bed roughness are reported all together along with the spatially averaged profile. In particular, Figures 4a and 4b report respectively the x- and y- velocity component in Run *1* (SB), Figures 4c and 4d similarly indicate x- and y- velocity component in Run *32* (GB) and finally Figures *4e* and *4f* refer to the x- and y- velocity component in Run *40* (RB). The velocity is made non-dimensional by means of the target current velocity, $U_{c,}$ obtained by dividing the flow rate for the cross section.

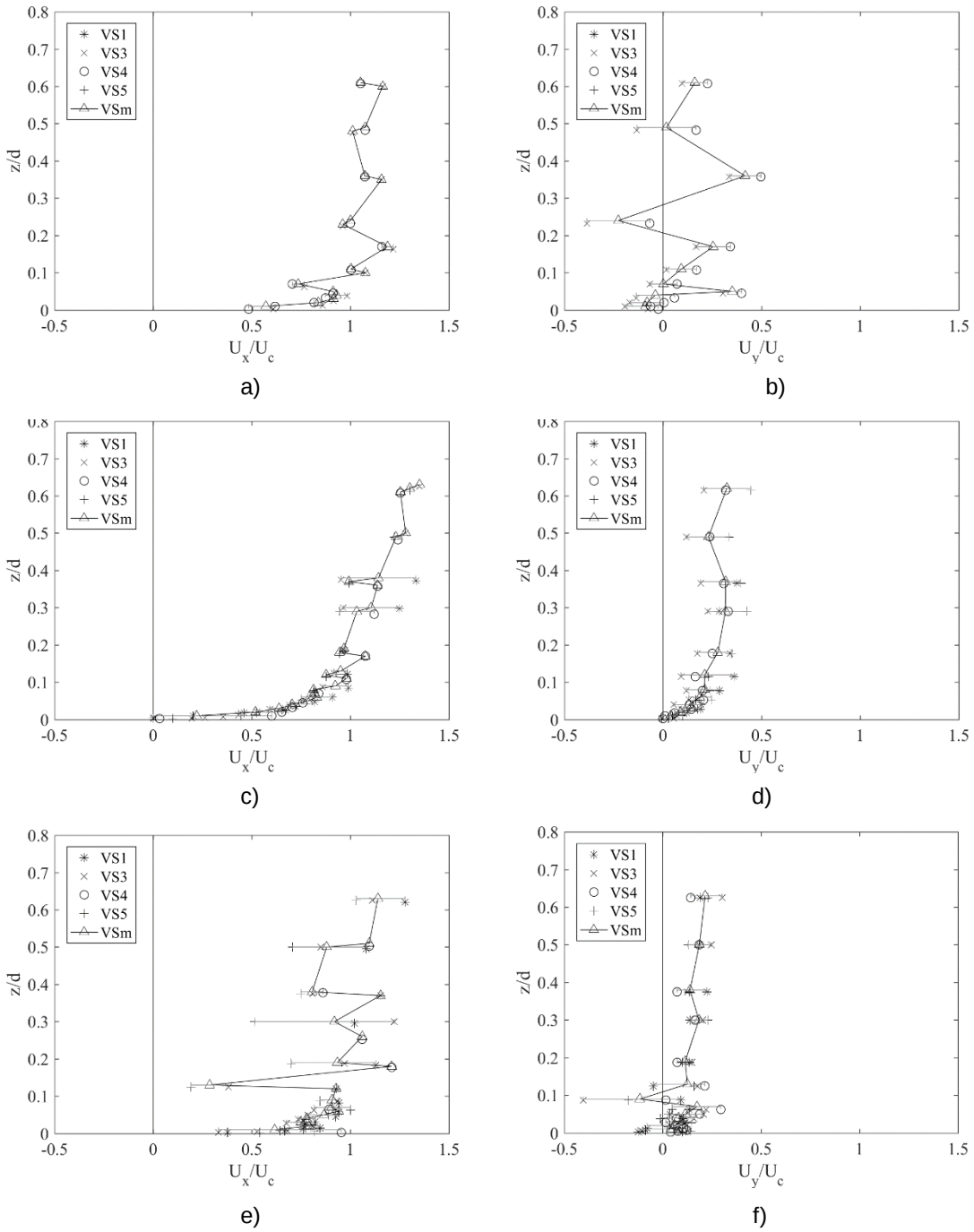

Figure 4. Mean velocity profiles acquired by the Vectrinos in the current only case (d=0.4 m): a) Run1 (CO, SB) Ux; b) Run1 (CO, SB) Uy c) Run32 (CO, GB) Ux; d) Run32 (CO, GB) Uy e) Run40 (CO, RB) Ux; f) Run40 (CO, RB) Uy.

It is possible to observe that in the SB case the measured U_x velocities are almost superimposed one over each other at all the measuring stations. The *y* component shows an irregular pattern which leads to argue the existence of transverse circulations inside the basin. In the GB case on the contrary, the scatter between each Vectrino Single Point is more relevant (up to 20% in the weak spot region), even though the averaged profile is less affected by abrupt changes.

The RB case shows an irregular pattern along the x component probably caused by a relevant transversal circulation maybe due also to the bed waviness close to bottom. Moreover, a significant variability among each Vectrino Single Point is also noted. For the y component of Run 40 the trend is more regular and the average profile shows a trend closer to each Vectrino Single Point.

In Figure 5 a current only, a wave only and a wave plus current conditions over three rough beds are plotted. Here respectively Run1, Run32 and Run40 (CO), Run3, Run36 and Run45 (WO),

Run7, Run34 and Run41 (WC) are considered *(d=0.4 m, H=0.12 m, T=2 s).* Each set of three velocity profiles refers to different bed roughness (SB, GB and RB).
While the wave only profile, as expected, shows only fluctuations around zero, the CO and WC profiles exhibit an increasing velocity from the bottom up to about *0.15-0.25 z/d.*
Here only the average profile is traced, while the spatial variability observed between the different Vectrino is represented in terms of an error bar. This variability is maximum at the bottom and is reduced far from the bed. It can be detected that, far from the bed, CO velocities are slightly higher than WC ones, while the opposite happens close to the bed. In the RB case however such behaviour is less clear.

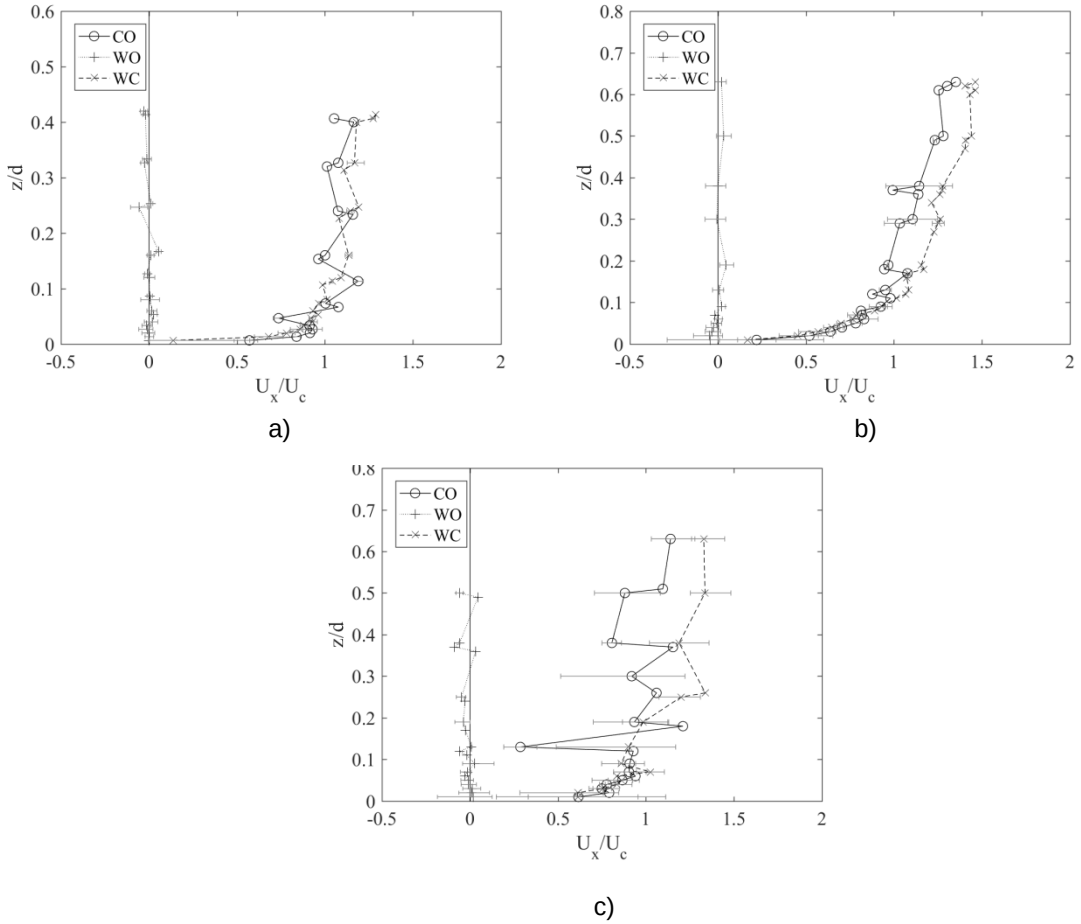

Figure 5. Velocity profiles along the *x* direction: a) SB case Run1 (CO), Run3 (WO), Run7(WC), b) GB case Run32 (CO), Run36 (WO), Run34 (WC), c) RB case Run40 (CO), Run45 (WO), Run41 (WC) d=0.4 m, H=0.12 m, T=2 s.

Along the y-direction (Figure 6) time averaged profiles show that in the case of wave only the mean velocity is negative for all SB, GB and RB case for the majority of the vertical profile due to the setting of the undertow current. The addition of the current onto the wave tends to compensate these two opposite flows, with a mean profile that shows velocities smaller than in the current only case.
As before, the variability observed between the different Vectrinos is represented in terms of an error bar. This variability in the lower part is more evident in the RB case (Figure 6c). This is probably related to the type of bed as it involves a greater measurement displacement between a measurement point and another; indeed, a strong difference arise between measurements taken on the crest and the trough; this effect is greatly reduced far away from the bed.
Plotting on a semi-logarithmic scale the acquired profiles, it is possible to recover the equivalent roughness k_s and the friction velocity u* respectively as 30 times the intercept and the angular coefficient of the log-layer. The latter quantity was used to determine the shear stress τ for the CO and WC conditions.
In Figure 7, the non-dimensional wall shear stress, obtained as the ratio of the wave-current shear stress to the current only one, is plotted versus the wave Reynolds number. Data are

grouped on the basis of the rough bed condition. The nondimensional shear stress undergoes a reduction for Reynolds numbers lower than approximately 5.000, i.e. the flow relaminarizes, as already observed by Lodahl et al (1998). This behaviour is typical of current dominated conditions. Then, for Reynolds numbers higher than 10.000 and wave dominated conditions, wave-current shear stress increases more than linearly with respect to the current only one. A similar behaviour was also found in Musumeci et al (2006) and in Faraci et al. (2008).

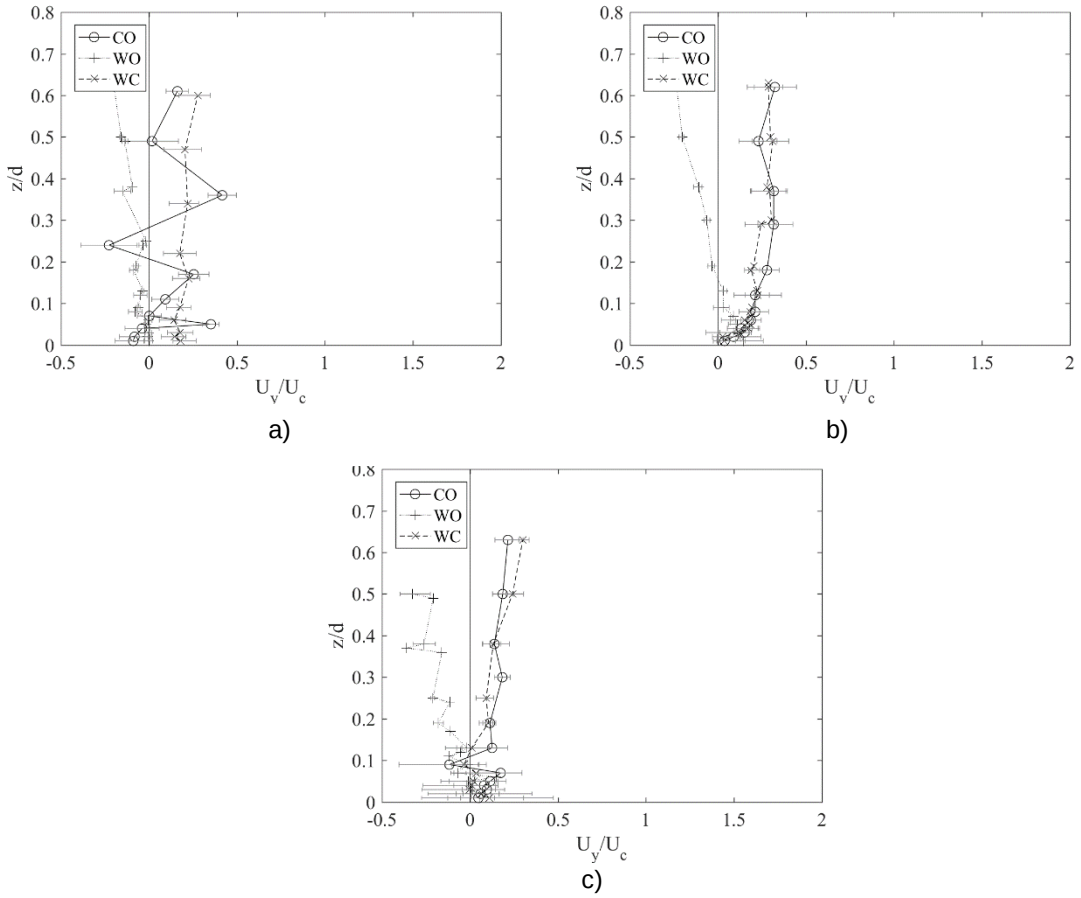

Figure 6. Velocity profiles along the *y* direction in the SB case, Run1 (CO), Run3 (WO), Run7 (WC) (a), GB case Run32 (CO), Run36 (WO), Run34 (WC), RB case Run40 (CO), Run45 (WO), Run41 (WC). d=0.4 m, H=0.12 m, T=2 s.

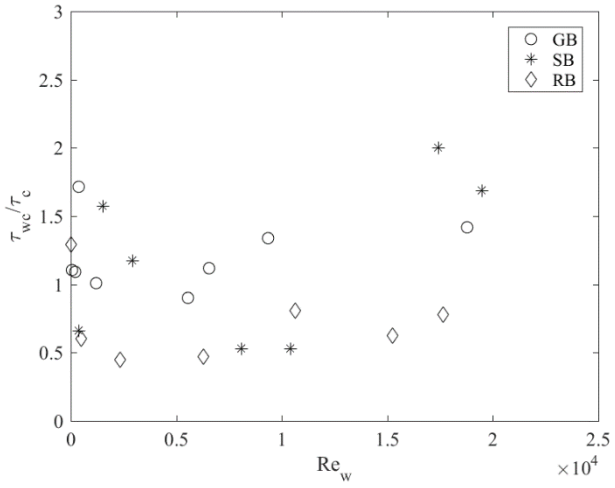

Figure 7. Non-dimensional wall shear stress as a function of wave Reynolds number.

5. CONCLUSIONS

This paper reports an overview of the first results obtained in the framework of the TA WINGS, funded by the EU through the Hydralab+ program. The project was aimed at gaining insights on orthogonal wave-current interaction over rough beds in both wave dominated and current dominated conditions. A detailed experimental campaign was performed in order to gather flow measurements in WO, CO and WC conditions over sand, gravel and rippled beds. The analyses of the velocity profiles revealed that far from the bed CO current directed velocities are slightly higher than WC ones, while the opposite happens close to the bed, except for the RB case where such behaviour is less perceptible. In the wave direction in the WO case, the mean velocity is negative for all the rough beds for the majority of the vertical profile, due to the setting of the undertow current. The addition of the current onto the wave tends to compensate these two opposite flows, with a mean profile that shows velocities smaller than in the current only case.
Finally, the nondimensional shear stress was also investigated, and a reduction for Reynolds numbers lower than approximately 5.000 was observed, i.e. the flow relaminarizes, as already observed by Lodahl et al (1998). This behaviour happens in current dominated conditions. Then, for Reynolds numbers higher than 10.000 and wave dominated conditions, wave-current shear stress increases more than linearly with respect to the current only one. A similar behaviour was also found in Musumeci et al (2006) and Faraci et al. (2008).

REFERENCES

Faraci, C., Foti, E., and Musumeci, R. (2008). Waves plus currents crossing at a right angle: the rippled bed case. J. of Geophys. Res., 113(C07018):1{26. doi: 10.1029/2007JC004468.

Faraci, C., Scandura, P., and Foti, E., (2015). Reflection of sea waves by combined caissons. J. Waterway, Port, Coast. and Ocean Eng., 141(2).

Faraci, C., Scandura, P., Musumeci, R., and Foti, E. (2018). Waves plus currents crossing at a right angle: near-bed velocity statistics. J. of Hydraulic Research, 56(4):464{481. doi: 10.1080/00221686.2017.1397557.

Fredsøe, J., Andersen, K. H., and Sumer, B. M. (1999). Wave plus current over a ripple-covered bed. Coastal Engineering, 38:177-221.

Goring, D. G. and Nikora, V. I. (2002). Despiking acoustic doppler velocimeter data. Journal of Hydraulic Engineering, 128(1):117-126.

Kemp, P. H. and Simons, R. R. (1982). The interaction between waves and turbulent current: waves propagating with current. J. of Fluid Mech., 116:227-250.

Kemp, P. H. and Simons, R. R. (1983). The interaction between waves and turbulent current: waves propagating against current. J. of Fluid Mech., 130:73-89.

Lodahl, C. R., Sumer, B. M., and Freds_e, J. (1998). Turbulent combined oscillatory ow and current in a pipe. J. of Fluid Mech., 373:313-348.

Musumeci, R. E., Cavallaro, L., Foti, E., Scandura, P., and Blondeaux, P. (2006). Waves plus currents crossing at a right angle. Experimental investigation. Journal of Geophysical Research, 111(C07). doi: 10.1029/2005JC002933.

van der Zanden, J., O'Donoghue, T., Hurther, D., C_aceres, I., McLelland, S. J., Ribberink, J. S., et al. (2017). Large-scale laboratory study of breaking wave hydrodynamics over a fixed bar. Journal of Geophysical Research: Oceans, 122(4):3287-3310.

Yoon, H.-D. and Cox, D. T. (2010). Large-scale laboratory observations of wave breaking turbulence over an evolving beach. Journal of Geophysical Research: Oceans, 115(C10).